International Journal of Astrobiology 16 (3): 237–243 (2017)
doi:10.1017/S1473550416000161

Ultraviolet irradiation of glycine in presence of pyrite as a model of chemical evolution: an experimental and molecular modelling approach

Azarhel de la Cruz-López[1,2], Ebelia del Ángel-Meraz[1], María Colín-García[3], Sergio Ramos-Bernal[2], Alicia Negrón-Mendoza[2] and Alejandro Heredia[2]

[1]*División Académica de Ingeniería y Arquitectura, Universidad Juárez Autónoma de Tabasco, Carretera Cunduacán-Jalpa de Méndez, Col. La Esmeralda. Cunduacán, C.P. 86690, Tabasco, México*
[2]*Universidad Nacional Autónoma de México, Instituto de Ciencias Nucleares, Ciudad Universitaria, Circuito Exterior S/N, Coyoacán, C.P. 04510, Ciudad de México, México e-mail: aheredia@nucleares.unam.mx*
[3]*Universidad Nacional Autónoma de México, Instituto de Geología, Ciudad Universitaria, Circuito Exterior S/N, Coyoacán, C.P. 04510 Ciudad de México, México*

Abstract: In this work, the molecular interaction of the amino acid glycine and the mineral pyrite was performed to gain insight into the potential role of the mineral as a precursor of chemical complexity in the presence of ultraviolet (UV) radiation. Glycine samples were self-assembled on pyrite with and without exposure to UV radiation and subsequently characterized by scanning electron microscopy, infrared spectroscopy (with the second-derivative method), and AM1 and PM3 semi-empirical molecular computational simulations. In this work, our molecular modelling results suggest that pyrite *acts* as a template for self-assembly of glycine, and it is a potential catalyst for the glycine dimerization of relevance in interstellar space and ancient Earth conditions. A change in the structural complexity of glycine from the α to its γ polymorph when irradiated with UV radiation can be a condition for chemical evolution towards living forms.

Received 24 November 2015, accepted 21 March 2016, first published online 26 July 2016

Key words: chemical evolution, glycine, pyrite, self-assembly, ultraviolet ionizing radiation.

Introduction

Mineral–organic interactions are of paramount relevance in the origins of life (Cleaves *et al.* 2012). The interaction of organics with different minerals is a source of chemical complexity (Colin-Garcia *et al.* 2012). Pyrite (FeS_2) is one of the most common sulphide minerals on the Earth. Geologic records indicate that banded iron formations dating from 3.9 Ga, representing probably the earliest sedimentary rocks, contain pyrite (Hazen *et al.* 2008). On Mars, the assemblage of goethite–jarosite–opal–clay observed was probably derived from the oxidation of iron-containing minerals (Burns & Fisher 1990; Zolotov & Shock 2005).

Specifically, the high-pressure reaction between FeS and H_2S (Rickard 2015) is identified as a primitive path for fixing carbon, through a chain of redox processes (Russell *et al.* 1994). In this chemical process, the elemental composition and crystalline structure of pyrite mineral (FeS_2) is of main significance (46.6% of Fe and 53.4% of S). For instance, the crystal system (cubic) of pyrite opens the way for coordination of organics in its sulphur-rich surface (Betejtin 1970). Pyrite is involved in CO_2 fixation in the presence of H_2S and was a potential catalyst in the primitive Earth towards synthesis of more complex molecules associated with the origins of living matter (Tributsch *et al.* 2003). Therefore, unravelling the potential chemical processes involved in small organics condensation and complexation will lead to a further understanding of the molecular mechanisms of prebiotic molecular evolution and how molecular and physicochemical inorganic aspects contributed to the origin of life (Cleaves *et al.* 2014).

Glycine ($NH_3^+CH_2COO^-$) is a low-molecular-weight and structurally simple molecule (75 g mol^{-1}) that might easily be synthesized in comet impact simulations (Goldman *et al.* 2010) and is found in other interstellar bodies, such as meteorites (Glavin & Bada 2001). Moreover, those interstellar bodies contain, among other solids, pyrite mineral (Moriarty *et al.* 2010). In primitive Earth studies, special emphasis must be paid to inorganics interacting with organics (Degens 1989) under different environmental conditions. Moreover, terrestrial planets such as Mars (Patel *et al.* 2004) and the primitive Earth, a lack of an ozone layer in the first stages was possible, having a strong ultraviolet (UV) irradiation as a potential driving force for chemical activation (Cockell 2000; Horneck 2007).

Many attempts have been made through different characterization methods in order to understand the molecular changes in glycine monomer, interacting with minerals of astrobiological relevance (Pilling *et al.* 2013) supporting the Oparin–Haldane hypothesis of chemical evolution (Okihana & Ponnamperuma 1982). To understand the mechanism of chemical evolution, infrared (IR) experimental methods and theoretical characterization studies are of main relevance (Baran & Ratajczak 2005; Contreras-Torres & Basiuk 2005). Here, we

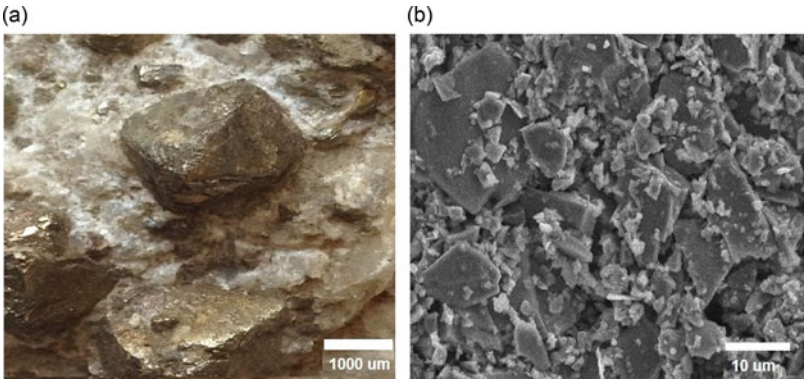

Fig. 1. Pyrite mineral showing its distinctive crystal habits (a) and a more detailed image (b) showing no furrows or sheets in the structure.

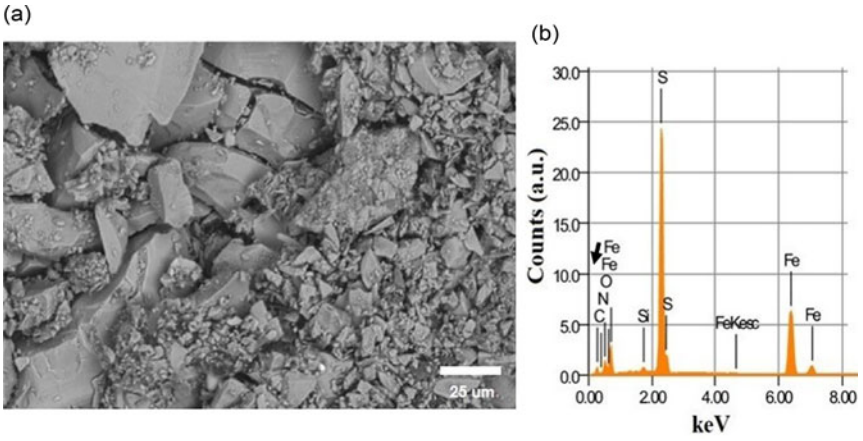

Fig. 2. SEM microphotograph of a characteristic sample of pyrite with self-assembled glycine (a) and the corresponding EDS analysis showing the presence of carbon (black arrow in b).

perform an experimental and theoretical study of the interaction of glycine with the mineral pyrite when the system is exposed to UV radiation. The aim was to figure out the molecular changes promoted by the mineral in the self-assembly of the amino acid as an example of a process of chemical evolution.

Materials and methods

Pyrite (Figs 1 and 2) was obtained from the collection of the Institute of Geology, UNAM and Rominmex S.A. de C.V. (Atlixco, Puebla, México), and glycine was obtained from Sigma-Aldrich (CAS-56-40-6). The pyrite sample was ground in an agate mortar and subsequently mixed with glycine solution (0.01 M) and left in the overnight up to dehydration. Solid solutions were performed with 0.2 g of mineral and put to interact with 0.5 ml of glycine solution. To maximize reproducibility, the same initial stock of ground pyrite was used for all the experimental procedures after it had been cleaned thoroughly in a series of acetone–distilled water–acetone–distilled water rinses. At least two repetitions per sample were performed to confirm the presence and consistency of bands. The precise frequencies of the different chemical groups were determined by cross-referencing against previously reported group-specific frequencies (Table 1).

Scanning electron microscopy (SEM) and energy-dispersive spectroscopy (EDS)

The SEM analysis was performed at the Laboratory of Analysis and Characterization (Academic Division of Engineering and Architecture UJAT-DAIA). The samples were analysed by SEM (Fig. 2(a)). For morphological analysis, the samples were mounted on conductive carbon tape in an aluminium sample holder. The samples were observed on the JEOL JSM-6010LA SEM (Japan), at 20 kV accelerating voltage under high vacuum. For the semi-quantitative and element composition energy dispersive detector (EDS) coupled to the SEM was employed (Fig. 2(b)). For processing the images, the InTouchScope™ software was used.

UV activation

Activation by UV light was performed with a mercury lamp (Pen ray UVP, UVC Light Sources, with fixed parameters, Cambridge, UK) with a primary energy being 254 nm (5.5 W m^{-2}), the irradiation period was 1 up to 24 h approximately, with intervals for manual mixing of the solid mixture. Analysis was performed over the different samples as follows (Table 1): pyrite (P), pyrite UV (PUV), glycine (G), glycine UV (GUV), pyrite–glycine (PG) and glycine–pyrite UV (PGUV).

https://doi.org/10.1017/S1473550416000161 Published online by Cambridge University Press

Table 1. *Assignment of detected attenuated total reflection-Fourier transform infrared spectroscopy (ATR-FTIR) frequencies of the different samples, pyrite (P), pyrite UV (PUV), glycine (G), glycine UV (GUV), pyrite–glycine (PG) and glycine–pyrite UV (PGUV). The assignment is based on the previously reported data*

Chemical group	P (cm^{-1})	PUV (cm^{-1})	G (cm^{-1})	GUV (cm^{-1})	PG (cm^{-1})	PGUV (cm^{-1})	References
COO^-	1211	668	694	694	663	1220	Pilling *et al.* (2013)
NH_3^+	1222	1218	892	892	1216	1458	Borda *et al.* (2004)
COOH	1243	1224	908	1033	1365	1505	Pilling *et al.* (2011)
CO–CH_3	1395	1388	1033	1331	1736	1974	Hu *et al.* (2012)
CH_3	1508	1737	1111	1407	2158	2157	Portugal *et al.* (2014)
CO_2	1560	1981	1131	1443	2070	2165	Cabán-Acevedo *et al.* (2014)
CO	1649	2179	1408	1500	2180	2173	Pilling *et al.* (2014)
NH_2	2161	2973	1500	1580	2158	2328	Rath *et al.* (2000)

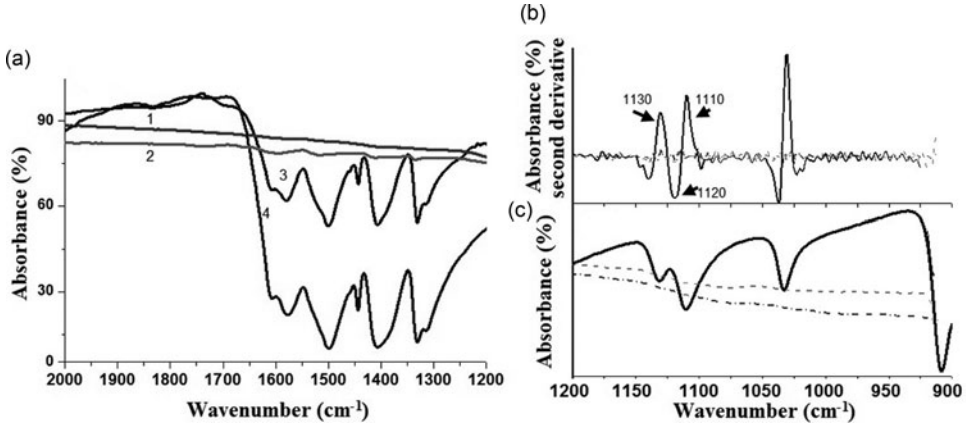

Fig. 3. (a) Characteristic ATR-FTIR spectra of glycine (1), glycine interacting with pyrite (2), UV-irradiated glycine interacting with pyrite (3), and (4) UV-irradiated glycine (see also Table 1 for the sampling strategy). The most clear-cut bands of the α-glycine indicated and were assigned to previously reported data (Table 1). (b) The second derivative method was used to confirm the presence of the α and γ glycine polymorphs, which are not seen directly in the FTIR (c).

ATR-FTIR spectroscopy

IR spectra were obtained by using an ATR-FTIR equipment (Spectrum 100 FTIR Spectrometer PerkinElmer, Waltham, Massachusetts) from 4000 to 650 cm^{-1} scan (over four scans). Analysis of the ATR-FTIR-obtained data, showed the typical bands for glycine and pyrite (Fig. 3(a) and (c)). The penetration depth of the laser beam in ATR-FTIR is about 2 μm making this method a proper technique for the analysis of surfaces (Mourant *et al.* 2003; Heredia *et al.* 2008). To perform a more detailed analysis, we used the method of the second derivative to determine most of the band positions (Fig. 3(b)). The second-derivative graphs have sharper peaks (bands) at the same frequency values, making their potential use of main significance during the analysis of fine details of IR spectra (for comparison see Fig. 3(a)–(c)).

Second-derivative method

Some steps are performed to investigate complex FTIR spectra, especially the overlapped bands. In order to gather all potential chemical and structurally useful information on the glycine and pyrite, the second-derivative step is used. This method involves band resolution enhancement. Here, the overlapping of bands are analysed by spectra differentiation. In general, all data points of the second derivative decrease in intensity in each derivative, but the relative resolutions are increased. The analysis of the second derivative and deconvolution of IR spectra were applied first in the early 1980s. Each method presented its own advantages for the exploration of the local changes in the spectra, although the theory and application of derivatives proved to be simpler. For some authors (Barth & Haris 2009), this advantage consists of a second derivative that is straightforward and requires no *a priori* knowledge of band parameters. An additional application of these procedures is that the solute concentration in the Beer–Lambert law (1) *lc* or in its second derivative (2) is not affected (Gallignani *et al.* 2014).

$$A(\tilde{\nu}) = \alpha(\tilde{\nu})lc, \tag{1}$$

$$\frac{d^2A(\tilde{\nu})}{d\tilde{\nu}^2} = \frac{d^2\alpha(\tilde{\nu})}{d\tilde{\nu}^2}lc. \tag{2}$$

Here, A is the wavenumber, $\bar{\nu}$ is the dependent absorbance, α is the wavenumber-dependent absorption coefficient, l is the section thickness, and c is the concentration.

Computational methods

Molecular modelling MM+ was performed starting with molecular mechanics and, afterwards, by semi-empirical quantum mechanics methods as implemented in the HyperChem

https://doi.org/10.1017/S1473550416000161 Published online by Cambridge University Press

Table 2. *Elemental composition (in %) of the pyrite samples with and without glycine*

Sample	C (%atom)	N (%atom)	S (%atom)	Fe (%atom)	C/N (%atom)	S/Fe (%atom)
Pyrite	35.3	n.a.	27.03	17.73	n.a.	1.52
Glycine–pyrite	42.55	6.34	25.48	16.24	6.7	1.56
Glycine–pyrite UV	30.57	1.64	31.40	20.55	18.64	1.52

n.a. not detected, glycine exposed to UV was not measured.

program Version 8.0 (HyperCube, Canada). Geometry optimizations were used to obtain the coordinates of molecular structures at potential energy minima (Colin-Garcia *et al.* 2014). Full geometry optimization of the organic and inorganic units were performed using the HyperChem settings for the MM+ force field, the Polak–Ribiere conjugate gradient algorithm, and a root-mean-square gradient (RMS) of 0.0001 kcal $Å^{-1}$ mol^{-1}. Molecular dynamics relaxation of the optimized structures was employed to look for possible local minima (step size of 0.001 ps, constant simulation temperature of 300 K and *ca.* 12 ps each model). The glycine model was obtained from the database in the software and edited to obtain the zwitterion and the geometrically optimized glycine structure to determine the most stable conformation (MM+ method). Glycine was chosen to solely interact with the pyrite unit with no water to simulate the simplest model of chemical activity.

The PM3 and AM1 semi-empirical methods

The optimized geometries that were obtained by the MM+ molecular mechanics method were further optimized with the PM3 and AM1 semi-empirical methods. In semi-empirical calculations, full geometry optimizations were performed on the restricted Hartree–Fock (RHF) basis, Polak–Ribiere conjugate gradient algorithm, and total RMS gradient of 0.0001 kcal $Å^{-1}$ mol^{-1}, as is suggested in the HyperChem manual, and mentioned previously as the most suitable methods for long biomolecules (Heredia *et al.* 2008).

Results and discussion

Scanning electron micrographs, optical microscope images and EDS results (Figs 2 and 3) show the morphological and chemical features of the pyrite and glycine samples. The EDS elemental relative content expressed as carbon/nitrogen (C/N) ratio shows no organic content after in-pyrite samples (Table 2). On the contrary, the C/N ratio content in the self-assembled glycine on pyrite 6.7%, whereas it is 18.64% in the pyrite with glycine irradiated with UV. This increment is probably due to the fact that the pyrite crystal stabilizes the glycine molecule on its surface (Table 2). The crystal in PGUV shows a remarkable content of glycine, as can be seen from the C/N ratio in Table 2.

The ATR-FTIR spectra revealed all the bands from glycine and pyrite (Fig. 3(a)) with a main composition of α-glycine (Fig. 3(b) and 4). After GUV irradiation, a change in intensities in the bands was noticeable (Fig. 4). The changes in the samples after irradiation appeared to originate from the UV activation of pyrite (Figs. 3(a) and 4) (Zhang *et al.* 2003). Already after UV irradiation, the bands were recognized as chemical changes, since their areas are influenced by UV activation (Fig. 3(b)). According to other theoretical studies, an intricate interaction among water molecules, mineral surfaces and glycine might be responsible for this behaviour (Folliet *et al.* 2013).

The ATR-FTIR spectra were collected from ground pyrite samples and further analysed to study the assembly and subsequent polymorph formation of glycine.

The spectra obtained displayed the most important fingerprints of glycine. The bands at $\sim$1131 cm^{-1} were assigned as rocking vibrations of NH_3^+ groups, and were clearly identified over all of the samples. For glycine irradiated in the UV, however, no clear changes were noticed, which is consistent with the chemical stability of glycine against the exposure to ionizing radiation; this is in agreement with earlier observations (Pernet *et al.* 2013). Other fingerprint bands that were absent in all spectra were those of amide I at $\sim$1650 cm^{-1} and amide II at $\sim$1550 cm^{-1} (black arrow in Fig. 4); these bands refer specifically to the peptide bonds. This shows that no dimerization of glycine units occurred.

The second derivative analysis of the ATR-FTIR spectra shows that the effects of UV irradiation are in bands near 1060 cm^{-1} (Fig. 4). In this region, there is a change in the band of glycine irradiated with UV, compared with the control sample. This result reveals a possible increase in glycine γ polymorph due to the importance of the activation generated by UV irradiation (dotted line, grey arrow in Fig. 4).

Computation simulations

To obtain insight into the viable molecular interactions between chemical groups from glycine to pyrite or glycine self-assembly, we have performed MM+ simulations. The combination of geometry optimization and molecular dynamics for establishing relaxation of the optimized structures, is useful to determine the local energy minima for every tested model (see Table 3) and represented graphically (see profile of heats of formation in Fig. 5). The most stable structure that was obtained was the model of −1832.52 kcal mol^{-1} corresponding to a semi-empirical method AM1 from 2GP unit (Table 3 cell in grey).

In this conformation, it was possible for glycine units to approach the Fe-rich regions (Fig. 6).

At the molecular scale, pyrite might interact with organics such as glycine through its thiol or iron surface sites rising to chemical reactivity (Bebié & Schoonen 2000).

https://doi.org/10.1017/S1473550416000161 Published online by Cambridge University Press

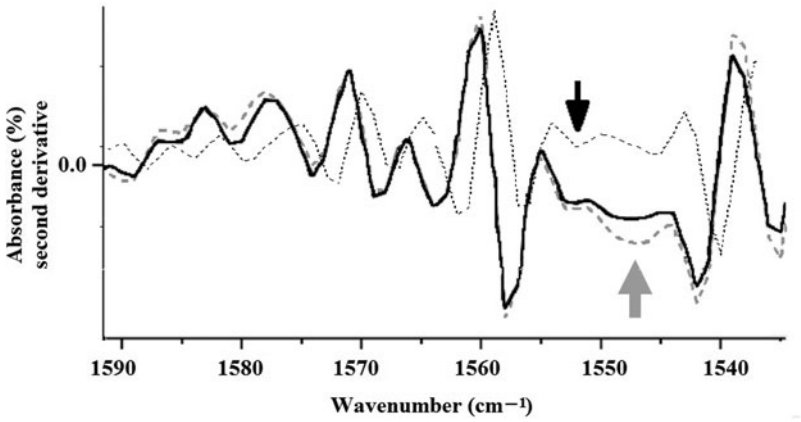

Fig. 4. Second-derivative ATR-FTIR of glycine (continuous line), UV treated glycine (dotted line) and GUV treated (discontinuous line) assembled in pyrite suggests a trend to transform glycine from α to γ polymorph (grey arrow). No amide bands (1560 and 1550 cm^{-1}) are present (black arrow).

Table 3. *Energies obtained from MM+ and semi-empirical procedures and the corresponding heats of formation from semi-empirical methods*

	Energies (kcal mol^{-1})			Heats of formation (kcal mol^{-1})	
	MM+	AM1	PM3	AM1	PM3
G	−0.09	−893.7	−897.07	−35.37	−34.91
G, G	−0.05	−1832.51	−1828.4	−71.88	−70.16
D(G–G)	−7.08	−1565.53	−1532.2	−24.3	−27.15
D(G–G)H_2O	−6.14	−1782.83	−1645.01	−85.85	−79.45
(G–G)H_2O	−3.26	−1771.33	−1749.23	−85.52	−80.06
GP	−3.04	−893.69	−897.07	−35.38	−34.94
2GP	−5.75	−1832.52	−1828.91	−99.17	−96.24
D(G–G)P	−8.92	−1809.25	−1752.12	−93.45	−91.21
D(G–G)H_2OP	−10.55	−1789.16	−1750.51	−23.3	−22.57

G, one unit of glycine; G,G, two units of zwitterionic glycine; D(G–G), glycine dipeptide; D(G–G)H_2O, glycine dipeptide with one molecule of water; (G–G)H_2O, two unites of zwitterionic glycine with one molecule of water; GP, one unit of glycine and one unit of pyrite; 2GP, two units of zwitterionic glycine and one unit of pyrite; D(G–G)P, glycine dipeptide in one unit of pyrite and D(G–G)H_2OP, glycine dipeptide and one unit of pyrite with one molecule of water.

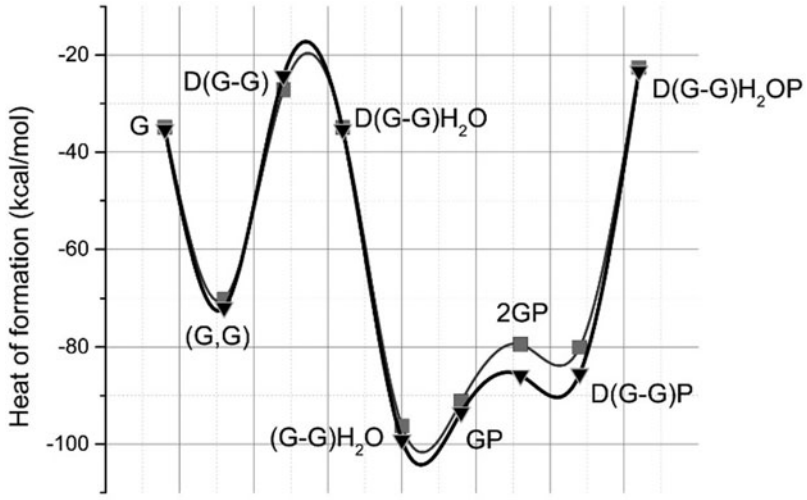

Fig. 5. Heats of formation from PM3 (■) and AM1 (▼) semi-empirical methods. Both semi-empirical methods, AM1 and PM3 result in favoured heats of formation for (G–G)H_2O, GP, 2GP and D(G–G)P molecules. So, it is important to note that using the method AM1, more heat of formation is shown, specifically for the 2GP molecule relative to the PM3 method.

https://doi.org/10.1017/S1473550416000161 Published online by Cambridge University Press

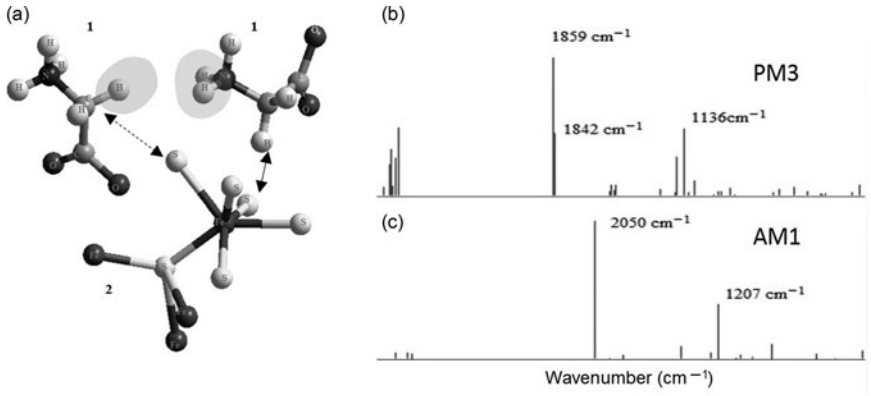

Fig. 6. Glycine molecules (1) interacting with a pyrite unit (2). (a) Two molecules of glycine interacting with the pyrite unit at the region close to the Fe–S bond. The distance between the chemical groups $–CH_2$ from glycine to S is 3.24 Å (arrow with discontinuous line) and 3.04 Å for the $–CH_2$ to S in another glycine molecule (arrow with solid line). The shortest distance between the two glycine molecules is 4.5 Å (shadowed regions). (b) PM3 and (c) AM1 IR simulations show clear-cut differences with the experimental results.

In the MM+ method, the glycine zwitterion was optimized. This conformation was, in addition, used for the semi-empirical methods. For this, two glycine molecules were put in the workspace to approach the regions of the unit of pyrite (Fig. 6).

The preliminary results have significance in prebiotic chemistry, specifically about the progressive increasing transformation from α to the γ glycine polymorph (a change in molecular packing) due to a non-biological mechanism. At the molecular scale, nonetheless, the possible glycine dimerization must be discussed in depth, since published works report the overwhelming stability of glycine under UV radiation (Okihana & Ponnamperuma 1982) and no polymerization under Co-60 radiation (Draganić *et al.* 1985). The role of water molecules in the heat of formation and the subsequent molecular transformation of glycine is of main importance. Specifically, the heat of formation in the AM1 and PM3 computer molecular simulations without water molecules favours the model in which two glycine molecules interact with pyrite (from Table 3, the difference in heats of formation between 2GP and D(G–G)P in AM1 corresponds to 5.76% and PM3 to 5.22%) over the glycine–glycine dimers. These results confirm that the lowest minima of heats of formation in the simulations favour the interaction of separated glycine units with pyrite in the absence of water molecules. Our ATR-FTIR further substantiates such observation, showing no peptide bonds (Figs. 3 and 4) under experimental conditions having water solutions (Fig. 3).

Simulated IR bands (Fig. 6(b) and (c)) show a divergence with the experimental ATR-FTIR that might originate in the lack of water molecules in the simulations. Besides, the computational model consists of single molecules, causing the local minima to produce just clear specific bands with no more complex molecular interactions. Although FTIR bands obtained here are not accurate, PM3 requires only a minor horizontal correction compared with the experimental results, and as such, might be used to explore the theoretical formation of the IR bands in future computational modelling efforts.

Conclusions

Here, the UV radiation was used as a driving force together with a mineral surface to impact the self-assembly of a specific amino acid polymorph. The mechanism of molecular interaction of glycine and pyrite is a matter of further investigation, although our computational simulations suggest a potential role of the complexation of sulphur-rich regions in the pyrite model. These preliminary results should be examined, thoroughly and additionally, under other radiation sources such as Co-60, and other physicochemical conditions (different pH, temperatures and pressures) that will lead to understand the prebiotic conditions of astrobiological importance capable of yielding amino acids polymorphs and oligomers. These new conditions will be studied at the molecular level by means of molecular simulations to understand the chemical complexity of prebiotic routes of complexation of molecules, important for living systems such as glycine. Molecular simulations of free radicals in heterogeneous systems (pyrite–glycine–water) and the use of γ radiation are of main relevance for these studies and are part of our current research.

Acknowledgements

ACL thanks Universidad Juárez Autónoma de Tabasco for the grant, and Dr Angel Meraz for supporting the Verano Científico program at ICN-UNAM under the advice of Dr Heredia. ACL also thanks co-workers of the Lab. of Chemical Evolution at Instituto de Ciencias Nucleares, UNAM for all the support. We thank Luciano Díaz González and Martín Cruz Villafañe for their technical support. We thank a lot the reviewers for the important improvements in our manuscript.

References

Baran, J. & Ratajczak, H. (2005). Polarised IR and Raman spectra of the γ-glycine single crystal. *Spectrochim. Acta A, Mol. Biomol. Spectrosc.* **61**, 1611–1626.

https://doi.org/10.1017/S1473550416000161 Published online by Cambridge University Press

Barth, A. & Haris, P.I. (2009). *Biological and Biomedical Infrared Spectroscopy*. IOS Press, Amsterdam, Netherlands.

Bebié, J. & Schoonen, M.A. (2000). Pyrite surface interaction with selected organic aqueous species under anoxic conditions. *Geochem. Trans.* **1**, 47.

Betejtin, A. (1970). *Curso de mineralogía*. Mir, Moscú.

Borda, M.J., Strongin, D.R. & Schoonen, M.A. (2004). A vibrational spectroscopic study of the oxidation of pyrite by molecular oxygen. *Geochim. Cosmochim. Acta* **68**, 1807–1813.

Burns, R.G. & Fisher, D.S. (1990). Iron-sulfur mineralogy of Mars: magmatic evolution and chemical weathering products. *J. Geophys. Res.* **95**, 14415.

Cabán-Acevedo, M., Kaiser, N.S., English, C.R., Liang, D., Thompson, B. J., Chen, H.-E., Czech, K.J., Wright, J.C., Hamers, R.J. & Jin, S. (2014). Ionization of High-density deep donor defect states explains the low photovoltage of iron pyrite single crystals. *J. Am. Chem. Soc.* **136**, 17163–17179.

Cleaves, H.J. II, Michalkova Scott, A., Hill, F.C., Leszczynski, J., Sahai, N., Hazen, R. (2012). Mineral–organic interfacial processes: potential roles in the origins of life. *Chem. Soc. Rev.* **41**, 5502.

Cleaves, H.J., Lazcano, A., Ledesma Mateos, I., Negrón-Mendoza, A., Peretó, J. & Silva, E. (2014). *Herrera's 'Plasmogenia' and Other Collected Works*. Springer New York, New York, NY.

Cockell, C.S. (2000). Ultraviolet radiation and the photobiology of earth's early oceans. *Orig. Life Evol. Biosph. J. Int. Soc. Stud. Orig. Life* **30**, 467–499.

Colin-Garcia, M., Heredia, A., Negron-Mendoza, A. & Ramos-Bernal, S. (2012). Organics-minerals interactions and the origin of life. *LPI Contrib.* **1667**, 6072.

Colin-Garcia, M., Heredia, A., Negron-Mendoza, A., Ortega, F., Pi, T. & Ramos-Bernal, S. (2014). Adsorption of HCN onto sodium montmorillonite dependent on the pH as a component to chemical evolution. *Int. J. Astrobiol.* **13**, 310–318.

Contreras-Torres, F.F. & Basiuk, V.A. (2005). Theoretical prediction of gas-phase infrared spectra of imidazo[1,2-a]pyrazinediones and imidazo [1,2-a]imidazo[1,2-d]pyrazinediones derived from glycine. *Spectrochim. Acta A, Mol. Biomol. Spectrosc.* **61**, 2560–2575.

Degens, E.T. (1989). *Perspectives on Biogeochemistry*. Springer, Berlin; Heidelberg; New York; London; Paris; Tokyo.

Draganić, Z.D., Niketić, V. & Vujošević, S.I. (1985). Radiation chemistry of an aqueous solution of glycine: compounds of interest to chemical evolution studies. *J. Mol. Evol.* **22**, 82–90.

Folliet, N., Gervais, C., Costa, D., Laurent, G., Babonneau, F., Stievano, L., Lambert, J.-F. & Tielens, F. (2013). A molecular picture of the adsorption of glycine in mesoporous silica through NMR experiments combined with DFT-D calculations. *J. Phys. Chem. C* **117**, 4104–4114.

Gallignani, M., Rondón, R.A., Ovalles, J.F. & Brunetto, M.R. (2014). Transmission FTIR derivative spectroscopy for estimation of furosemide in raw material and tablet dosage form. *Acta Pharm. Sin. B* **4**, 376–383.

Glavin, D.P. & Bada, J.L. (2001). Survival of amino acids in micrometeorites during atmospheric entry. *Astrobiology* **1**, 259–269.

Goldman, N., Reed, E.J., Fried, L.E., William Kuo, I.F. & Maiti, A. (2010). Synthesis of glycine-containing complexes in impacts of comets on early Earth. *Nat. Chem.* **2**, 949–954.

Hazen, R.M., Papineau, D., Bleeker, W., Downs, R.T., Ferry, J.M., McCoy, T.J., Sverjensky, D.A. & Yang, H. (2008). Mineral evolution. *Am. Mineral.* **93**, 1693–1720.

Heredia, A., van der Strate, H.J., Delgadillo, I., Basiuk, V.A. & Vrieling, E. G. (2008). Analysis of organo–silica interactions during valve formation in synchronously growing cells of the diatomnavicula pelliculosa. *ChemBioChem* **9**, 573–584.

Horneck, G. (ed.) (2007). *Complete Course in Astrobiology*. Wiley–VCH, Weinheim.

Hu, J., Zhang, Y., Law, M. & Wu, R. (2012). Increasing the band gap of iron pyrite by alloying with oxygen. *J. Am. Chem. Soc.* **134**, 13216–13219.

Moriarty, D., Hibbitts, C.A., Lisse, C.M., Dyar, M.D., Harlow, G., Ebel, D. & Peale, R. (2010). Near-far IR spectra of sulfide minerals relevant to comets. In *Presented at the Lunar and Planetary Science Conf.*, March 1–5, 2010 in The Woodlands, Texas, p. 2447.

Mourant, J.R., Yamada, Y.R., Carpenter, S., Dominique, L.R. & Freyer, J.P. (2003). FTIR spectroscopy demonstrates biochemical differences in mammalian cell cultures at different growth stages. *Biophys. J.* **85**, 1938–1947.

Okihana, H. & Ponnamperuma, C. (1982). A protective function of the coacervates against UV light on the primitive Earth. *Nature* **299**, 347–349.

Patel, M.R., Bérces, A., Kerékgyárto, T., Rontó, G., Lammer, H. & Zarnecki, J.C. (2004). Annual solar UV exposure and biological effective dose rates on the Martian surface. *Adv. Space Res. Off. J. Comm. Space Res. COSPAR* **33**, 1247–1252.

Pernet, A., Pilmé, J., Pauzat, F., Ellinger, Y., Sirotti, F., Silly, M., Parent, P. & Laffon, C. (2013). Possible survival of simple amino acids to X-ray irradiation in ice: the case of glycine. *Astron. Astrophys.* **552**, A100.

Pilling, S. *et al.* (2011). Photostability of gas- and solid-phase biomolecules within dense molecular clouds due to soft X-rays: photostability of biomolecules in ISM. *Mon. Not. R. Astron. Soc.* **411**, 2214–2222.

Pilling, S., Mendes, L.A.V., Bordalo, V., Guaman, C.F.M., Ponciano, C.R. & da Silveira, E.F. (2013). The influence of crystallinity degree on the glycine decomposition induced by 1 mev proton bombardment in space analog conditions. *Astrobiology* **13**, 79–91.

Pilling, S., Nair, B.G., Escobar, A., Fraser, H. & Mason, N. (2014). The temperature effect on the glycine decomposition induced by 2 keV electron bombardment in space analog conditions. *Eur. Phys. J. D* **68**, 1–9.

Portugal, W., Pilling, S., Boduch, P., Rothard, H. & Andrade, D.P.P. (2014). Radiolysis of amino acids by heavy and energetic cosmic ray analogues in simulated space environments: glycine zwitterion form. *Mon. Not. R. Astron. Soc.* **441**, 3209–3225.

Rath, R.K., Subramanian, S. & Pradeep, T. (2000). Surface chemical studies on pyrite in the presence of polysaccharide-based flotation depressants. *J. Colloid Interface Sci.* **229**, 82–91.

Rickard, D. (2015). *Pyrite: A Natural History of Fool's Gold*. Oxford University Press, New York.

Russell, M.J., Daniel, R.M., Hall, A.J. & Sherringham, J.A. (1994). A hydrothermally precipitated catalytic iron sulphide membrane as a first step toward life. *J. Mol. Evol.* **39**, 231–243.

Tributsch, H., Fiechter, S., Jokisch, D., Rojas-Chapana, J. & Ellmer, K. (2003). Photoelectrochemical power, chemical energy and catalytic activity for organic evolution on natural pyrite interfaces. *Orig. Life Evol. Biosph. J. Int. Soc. Stud. Orig. Life* **33**, 129–162.

Zhang, X., Borda, M.J., Schoonen, M.A. & Strongin, D.R. (2003). Pyrite oxidation inhibition by a cross-linked lipid coating. *Geochem. Trans.* **4**, 8.

Zolotov, M.Y. & Shock, E.L. (2005). Formation of jarosite-bearing deposits through aqueous oxidation of pyrite at Meridiani Planum. *Mars. Geophys. Res. Lett.* **32**. doi: 10.1029/2005GL024253.